A unified approach to acoustical reflection imaging. II: The inverse problem

A. J. Berkhout and C. P. A. Wapenaar
Delft University of Technology, Laboratory of Seismics and Acoustics, P.O. Box 5046, 2600 GA Delft, The Netherlands

(Received 20 December 1990; accepted for publication 19 October 1992)

Using the forward matrix model, as derived in part I [A. J. Berkhout, J. Acoust. Soc. Am. **93**, 2005–2016(1993)], it is shown that the first and main part of numerical acoustic imaging consists of a wave field extrapolation process by double matrix inversion. Physically, the wave field extrapolation process means that the downward propagation effects and the upward propagation effects are eliminated from the measurements. Next, the reflection information is extracted from the wave field extrapolation result. Optionally, the reflection information is translated to discipline-oriented material parameters by some data fitting process. Double focusing, i.e., focusing in emission and focusing in detection, is closely related to the above numerical imaging process. Finally, it is shown that imaging of zero-offset or puls-echo data can be formulated by single matrix inversion, involving phase shifts only.

PACS numbers: 43.60.Gk, 43.60.Pt

INTRODUCTION

In part I of this paper (Berkhout, 1993) a general forward model has been derived for discrete acoustic reflection data:

$$\mathbf{P}^-(z_0) = \left(\sum_{m=1}^{M} \mathbf{W}^-(z_0,z_m)\mathbf{R}^+(z_m)\mathbf{W}^+(z_m,z_0) \right) \times \mathbf{S}^+(z_0), \tag{1a}$$

with

$$\mathbf{S}^+(z_0) = \mathbf{D}^+(z_0)\mathbf{S}(z_0), \tag{1b}$$

$$\mathbf{P}(z_0) = \mathbf{D}^-(z_0)\mathbf{P}^-(z_0). \tag{1c}$$

In expressions (1a)–(1c) two corresponding columns in the source matrix $\mathbf{S}$ (or $\mathbf{S}^+$) and measurement matrix $\mathbf{P}$ (or $\mathbf{P}^-$) refer to one experiment. Matrix operators $\mathbf{D}^+$ and $\mathbf{D}^-$ are defined by the boundary conditions at the data acquisition surface ($z = z_0$) as well as the choice of sources and detectors (velocity and/or pressure). Propagation matrices $\mathbf{W}^+$ and $\mathbf{W}^-$ define the propagation effects in the measurements; reflection matrix $\mathbf{R}^+$ defines the (angle-dependent) reflection effects in the measurements. All matrices refer to one Fourier component (frequency domain formulation). The choice of a *frequency* domain formulation has the important consequence that the multi-dimensional forward model (1a) is relatively simple. To keep the notation simple as well, the frequency parameter ω has been omitted. Note that in one-dimensional media all matrices simplify to Toeplitz matrices and *matrix* equation (1) can be rewritten as a *scalar* equation in the spatial Fourier domain:

$$\tilde{P}^-(\mathbf{k}_r,\mathbf{k}_s,z_0,\omega) = \sum_{m=1}^{M} [\tilde{W}^-(\mathbf{k}_r,\Delta z_m,\omega)\tilde{R}^+(\mathbf{k}_r,\mathbf{k}_s,z_m,\omega) \times \tilde{W}^+(\mathbf{k}_s,\Delta z_m,\omega)]\tilde{S}^+(\mathbf{k}_s,z_0,\omega) \tag{1d}$$

with $\Delta z_m = (z_m - z_0)$, $\mathbf{k} = (k_x,k_y)$, subscript s referring to the source coordinate, and subscript r referring to the receiver coordinate.

In part I multiple scattering caused by the surface has been simply introduced by using in (1a):

$$\mathbf{P}^+(z_0) = \mathbf{S}^+(z_0) + \mathbf{R}^-(z_0)\mathbf{P}^-(z_0) \tag{2}$$

instead of $\mathbf{S}^+(z_0)$, where $\mathbf{R}^-(z_0)$ defines the surface reflectivity for upward traveling waves. Expression (2) has also been generalized for *internal* multiple scattering.

The objective of the proposed forward model is not primarily for simulation purposes (there exist excellent finite difference and finite element algorithms for acoustic simulation). The primary objective of our version of the forward model is the derivation of a generalized acoustic *imaging* and *inversion* process. We will see that our formulation in terms of matrix operators is pre-eminently suited for the derivation and understanding of imaging and inversion methods.

In the *forward* problem all details about the data acquisition procedure are known, the acoustic properties of the surface and medium (trend *and* detail) are available, and the measurements need to be computed ("numerical simulation"). In the case where we start with reflectivity, simulation means

$$\mathbf{R}^+(z) \rightarrow \mathbf{P}(z_0). \tag{3a}$$

In the *inverse* problem, all details about the data acquisition procedure should be known, the measurements are available, and the medium parameters need to be computed. If the spatial reflectivity distribution is aimed for (reflection imaging), inversion means

$$\mathbf{P}(z_0) \rightarrow \mathbf{R}^+(z). \tag{3b}$$

Generally, in reflection imaging the *diagonal* elements of $\mathbf{R}^+(z)$ are computed only, meaning that the *angle-dependence* information of reflection is not aimed for (one reflection coefficient per medium grid point).

For a high-resolution result the *localization* (position-

ing) information can be supplemented with *shape* and *size* information. In addition, if *all* elements of the reflection matrix are computed, then for each grid point *angle-dependent* reflection information is available as well and reflection imaging can be followed by the computation of the material parameters (post processing):

$$\mathbf{R}^+(z) \rightarrow \boldsymbol{\rho}(z), \mathbf{c}_p(z), \mathbf{c}_s(z), \tag{3c}$$

where $\boldsymbol{\rho}(z)$, $\mathbf{c}_p(z)$, $\mathbf{c}_s(z)$ are diagonal matrices that represent, respectively, density, longitudinal velocity, and shear velocity (if applicable) at each grid point of depth level z. In most imaging techniques results are *not* in terms of material parameters but are in terms of local reflectivity (reflection imaging).

I. IMAGE FORMATION BY DOUBLE INVERSION

If we ignore for the moment the influence of the surface on the measurements and we assume perfect dipole sources and pressure detectors $[\mathbf{D}^+(z_0) = \mathbf{D}^-(z_0) = \mathbf{S}^+(z_0) = \mathbf{I}]$, then the forward model (1a) simplifies to

$$\mathbf{P}(z_0) = \mathbf{X}(z_0, z_0)$$

with

$$\mathbf{X}(z_0, z_0) \approx \sum_{m=1}^{M} \mathbf{W}^-(z_0, z_m)\mathbf{R}^+(z_m)\mathbf{W}^+(z_m, z_0).$$

If the objective of reflection imaging involves estimation of $\mathbf{R}^+(z_m)$, it can be seen from the above expression that the downward propagation effects from z_0 to z_m and the upward propagation effects from z_m to z_0 need be compensated. Or, in mathematical terms, the propagation matrices $\mathbf{W}^+(z_m, z_0)$ and $\mathbf{W}^-(z_0, z_m)$ need be inverted:

$$\mathbf{X}(z_m, z_m) = \mathbf{F}^-(z_m, z_0)\mathbf{X}(z_0, z_0)\mathbf{F}^+(z_0, z_m) \tag{4a}$$

with

$$\mathbf{F}^-(z_m, z_0) = [\mathbf{W}^-(z_0, z_m)]^{-1} \approx [\overline{\mathbf{W}}^+(z_m, z_0)]^* \tag{4b}$$

$$\mathbf{F}^+(z_0, z_m) = [\mathbf{W}^+(z_m, z_0)]^{-1} \approx [\overline{\mathbf{W}}^-(z_0, z_m)]^*, \tag{4c}$$

where $\overline{\mathbf{W}}$ is based on the macro model and where * denotes complex conjugation.

In the seismic exploration inversion process (4a) is generally referred to as "redatuming." From (4a) it follows that the elements of $\mathbf{X}(z_m, z_m)$ can be written as

$$X_{ij}(z_m, z_m) = \sum_k \sum_l F^-_{ik}(z_m, z_0) X_{kl}(z_0, z_0) F^+_{lj}(z_0, z_m) \tag{5a}$$

or, if we are interested in the diagonal elements only,

$$X_{ii}(z_m, z_m) = \sum_k \sum_l F^-_{ik}(z_m, z_0) X_{kl}(z_0, z_0) F^+_{li}(z_0, z_m). \tag{5b}$$

In practical solutions one generally chooses

$$F^-_{ik}(z_m, z_0) = [\overline{W}^+_{ik}(z_m, z_0)]^*,$$

$$F^+_{lj}(z_0, z_m) = [\overline{W}^-_{lj}(z_0, z_m)]^*,$$

which is consistent with the suggested approximations in (4b) and (4c).

Note that for one-dimensional macro models numerical image formation involves a double deconvolution process. Figure 1 gives a schematical illustration.

After the double inversion process (4) has been completed for all Fourier components of interest, reflectivity matrix $\mathbf{R}^+(z_m)$ needs to be computed from $\mathbf{X}(z_m, z_m)$. First, let us look at the Radon transform of one row of $\mathbf{X}(z_m, z_m)$:

$$\tilde{X}(x_i, z_m, \omega; p) = \sum_k X_{ik}(z_m, z_m) e^{+j\omega(x_i - x_k)p}, \tag{6a}$$

where p is the ray parameter.

Expression (6a) represents the response of the medium at grid point (x_i, z_m) *in terms of plane waves*. Realizing that the inversion operators $\mathbf{F}^-$ and $\mathbf{F}^+$ remove the propagation effects (travel time and geometrical spreading) from the measurements, the contribution of the inhomogeneities at z_m in $\tilde{X}(x_i, z_m, \omega; p)$ can be found at $t = 0$, the contribution from deeper depth levels $(z > z_m)$ can be found at positive times and the contribution from shallower depth levels $(z < z_m)$ can be found at negative times. Hence,

$$\tilde{R}^+(x_i, z_m; p) = \frac{1}{N} \sum_{n=1}^{N} \tilde{X}(x_i, z_m, \omega_n; p) \tag{6b}$$

represents the angle-dependent reflection coefficient at grid point (x_i, z_m). Note that the inverse Fourier transform $(\omega \rightarrow t = 0)$, as given in (6b), may also be considered as an *averaging* process where all contributions from $z \neq z_m$ are averaged away. In practical situations averaging will occur over a limited frequency range only, and *weighted* averaging

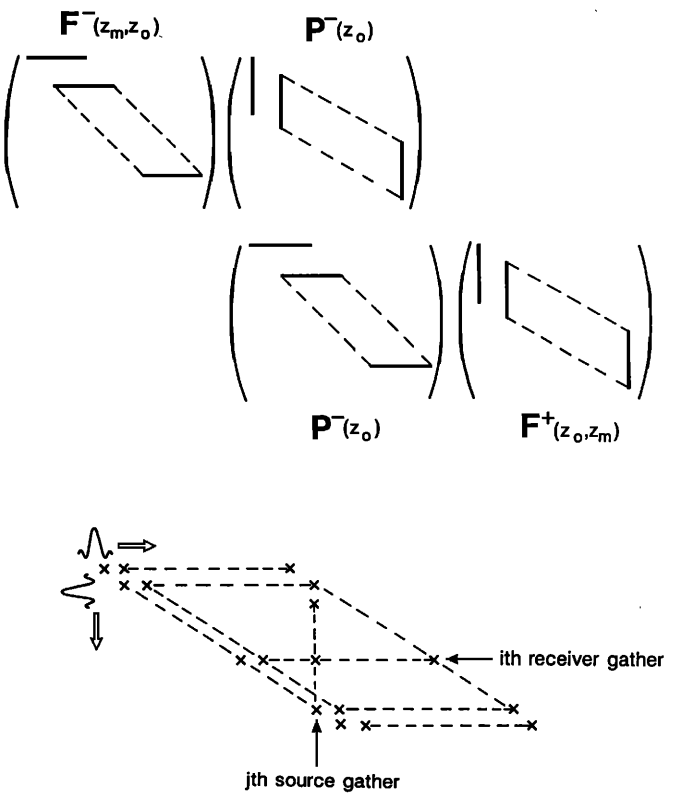

FIG. 1. Image formation involves double matrix inversion or, for one-dimensional media, a double deconvolution process along the source and receiver coordinate.

may be applied (noise considerations). Of course, the less frequencies contribute to the average, the more the influence from other depth levels (resolution considerations).

Now, the reflection matrix elements for one Fourier component follow directly from (6b) by inverse Radon transformation

$$R_{ik}^{+}(z_m) = \frac{1}{L}\sum_{l=1}^{L} \tilde{R}^{+}(x_i,z_m;p_l)e^{-j\omega(x_i-x_k)p_l}, \quad (6c)$$

where L is the number of ray parameters. Reflection coefficients $\tilde{R}^{+}(x_i,z_m;p_l)$ and matrix elements $R_{ik}^{+}(z_m)$ are alternative presentations for the angle-dependent reflection property at (x_i,z_m).

Note from (6c) that each diagonal element of the reflectivity matrix equals an *average* reflection coefficient

$$R_{ii}^{+}(z_m) = \frac{1}{L}\sum_{l=1}^{L} \tilde{R}^{+}(x_i,z_m;p_l). \quad (6d)$$

Note also that $R_{ii}^{+}(z_m)$ can be easily computed directly from redatuming result $\mathbf{X}(z_m,z_m)$:

$$R_{ii}^{+}(z_m) = \frac{1}{N}\sum_{n=1}^{N} X_{ii}(z_m,z_m), \quad (6e)$$

where the diagonal element $X_{ii}(z_m,z_m)$ represents one Fourier component (frequency ω_n) of the zero-offset (pulse-echo) response at grid point (x_i,z_m). As mentioned before, $R_{ii}^{+}(z_m)$ is the quantity that is generally aimed for in conventional reflection imaging.

In seismic exploration image formation by double inversion according to (5b) and averaging according to (6e) is called "seismic migration."

II. IMAGE FORMATION BY DOUBLE FOCUSING

In the aforegoing, numerical image formation was achieved by eliminating the influence of the propagation matrices $\mathbf{W}^{+}$ and $\mathbf{W}^{-}$ from $\mathbf{P}(z_0)$ in a separate data processing step, yielding the (angle-dependent) reflection properties at each lateral position of depth level z_m as quantified by reflection matrix $\mathbf{R}^{+}(z_m)$.

In the following an alternative approach is followed by designing the source array and detector array such that a reflection image is directly obtained as part of the data acquisition step.

(1) Choose the ith column of $\mathbf{S}^{+}(z_0)$, i.e., the source array at lateral position x_i, according to column vector $\mathbf{S}_i^{+}(z_0)$ such that

$$\mathbf{I}_i = \mathbf{W}^{+}(z_m,z_0)\mathbf{S}_i^{+}(z_0), \quad (7a)$$

where $\mathbf{I}_i = e^{-j\omega\bar{\tau}_m}(0,...,0,1,0,...,0)^T$ with $\bar{\tau}_m$ being the average vertical travel time between the surface and the mth level. This means that with the ith experiment the ith lateral position of depth level z_m is illuminated only. Therefore, (7a) quantifies focusing at emission [Fig. 2(a)].

(2) Choose the ith row of $\mathbf{D}^{-}(z_0)$, i.e., the detector array at lateral position x_i, according to row vector $\mathbf{D}_i^{-}(z_0)$ such that

$$\mathbf{I}_i^T = \mathbf{D}_i^{-}(z_0)\mathbf{W}^{-}(z_0,z_m). \quad (7b)$$

This means that with the ith experiment only the information of the ith lateral position of depth level z_m is received. Therefore, (7b) quantifies focusing at reception [Fig. 2(b)].

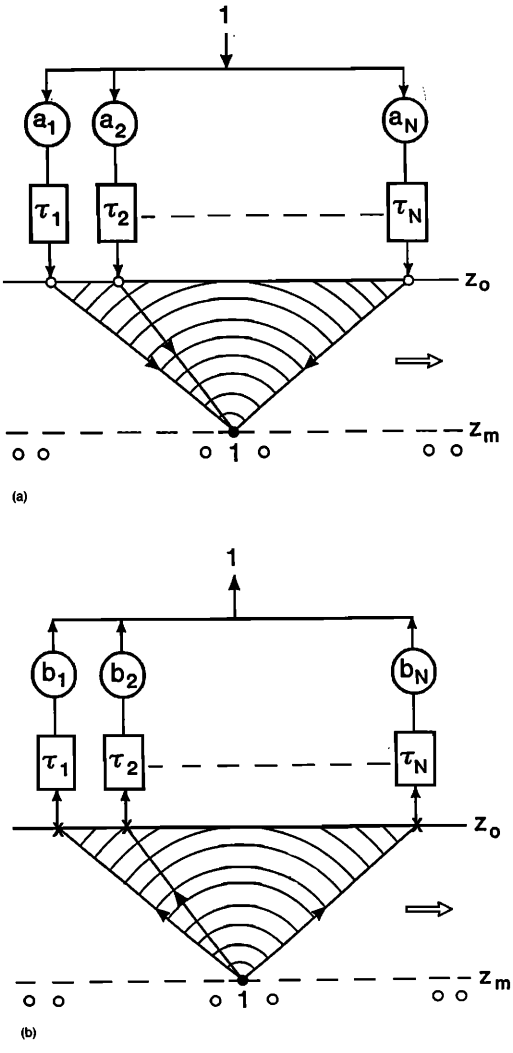

FIG. 2. (a) Generalized focusing in emission; (b) generalized focusing in detection.

One double focusing experiment according to (7a) and (7b) yields for the inhomogeneities at z_m:

$$\begin{aligned} X_{ii}(z_0,z_0) &= \mathbf{D}_i^{-}(z_0) \times\left(\sum_{h=1}^{M}\mathbf{W}^{-}(z_0,z_h)\mathbf{R}^{+}(z_h)\mathbf{W}^{+}(z_h,z_0)\right)\mathbf{S}_i^{+}(z_0) \\ &= [\mathbf{D}_i^{-}(z_0)\mathbf{W}^{-}(z_0,z_m)]\mathbf{R}^{+}(z_m) \times[\mathbf{W}^{+}(z_m,z_0)\mathbf{S}_i^{+}(z_0)] + \epsilon(z\neq z_m) \\ &= \mathbf{I}_i^T\mathbf{R}^{+}(z_m)\mathbf{I}_i + \epsilon(z\neq z_m) \\ &= R_{ii}^{+}(z_m)e^{-2j\omega\bar{\tau}_m} + \epsilon(z\neq z_m) \end{aligned} \quad (8a)$$

or, after inverse Fourier transformation for $t = 2\bar{\tau}_m$ ("averaging"),

$$\hat{R}_{ii}^{+}(z_m) = \frac{1}{N}\sum_{n=1}^{N} X_{ii}(z_0,z_0)e^{2j\omega_n\bar{\tau}_m}. \quad (8b)$$

In (8b) the contribution of

$$\frac{1}{N}\sum_{n=1}^{N}\epsilon(z\neq z_m)e^{2j\omega_n\bar{\tau}_m}$$

represents the effect of limited resolution.

Note that, apart from resolution problems, the partially focused contribution from inhomogeneities at $z<z_m$ can be found at $t<2\bar{\tau}_m$; the partially focused contribution from inhomogeneities at $z>z_m$ can be found at $t>2\bar{\tau}_m$. Note also the similarity of (8b) and (6e).

The experiment should be repeated for each lateral position and for each depth level of interest.

III. IMAGE FORMATION FOR ZERO OFFSET DATA

In part I (Berkhout, 1993) we have shown that the model of zero offset data (pulse-echo data) can be formulated as

$$\mathbf{P}_0^-(z_0)=\sum_{m=1}^{M}\mathbf{W}_0(z_0,z_m)\mathbf{R}_0^+(z_m), \tag{9}$$

where $\mathbf{P}_0^-(z_0)$ contains the diagonal elements of $\mathbf{P}^-(z_0)$, $\mathbf{R}_0^+(z_m)$ contains the zero offset reflection coefficients at z_m and the elements of $\mathbf{W}_0(z_0,z_m)$ contain the product of the related elements of $[\mathbf{W}^+(z_m,z_0)]^T$ and $\mathbf{W}^-(z_0,z_m)$.

It can be easily seen from (9) that redatuming of zero offset data involves only *one* matrix inversion per depth level

$$\mathbf{P}_0^-(z_m)=\mathbf{F}_0(z_m,z_0)\mathbf{P}_0^-(z_0) \tag{10a}$$

with

$$\mathbf{F}_0(z_m,z_0)=[\mathbf{W}_0(z_0,z_m)]^{-1}, \tag{10b}$$

the inversion being carried out in some stable sense.

Computation of the zero-offset reflection coefficients simplifies to

$$R_0^+(x_i,z_m)=\frac{1}{N}\sum_{n=1}^{N}P_0^-(x_i,z_m,\omega_n). \tag{11}$$

For the evaluation of $[\mathbf{W}_0(z_0,z_m)]^{-1}$ let us consider a homogeneous medium. For a homogeneous medium with dipole sources and pressure detectors one row of $\mathbf{W}_0(z_0,z_m)$ is defined by (far-field expressions):

$$W_0(x,\Delta z_m,\omega)=W^2(x,\Delta z_m,\omega)=\frac{jk}{2\pi}\frac{\cos^2\phi}{r}e^{-2jkr}\quad(2D), \tag{12a}$$

$$W_0(x,y,\Delta z_m,\omega)=W^2(x,y,\Delta z_m,\omega)=\left(\frac{jk}{2\pi}\right)^2\frac{\cos^2\phi}{r^2}e^{-2jkr}\quad(3D) \tag{12b}$$

with $k=\omega/c$, $r=\sqrt{x^2+\Delta z_m^2}$ (2D) or $r=\sqrt{x^2+y^2+\Delta z_m^2}$ (3D) and $\cos\phi=\Delta z_m/r$. Note from (12a) and (12b) the important property that the time delays in W_0 equal the time delays in $W^-(=W^+)$ if the velocity c is replaced by $c/2$.

Vector equation (9) can be rewritten in the spatial Fourier domain as a scalar equation

$$\tilde{P}_0^-(\mathbf{k},z_0,\omega)=\sum_{m=1}^{M}\tilde{W}_0(\mathbf{k},\Delta z_m,\omega)\tilde{R}_0^+(\mathbf{k},z_m,\omega), \tag{13a}$$

where $\mathbf{k}=(k_x,0)$ for 2D and $\mathbf{k}=(k_x,k_y)$ for 3D.

Using the stationary phase approach for the spatial Fourier transform we obtain

$$\tilde{W}_0(\mathbf{k},\Delta z_m,\omega)=\frac{c/2}{\omega}\sqrt{\frac{jk_z^3}{8\pi\Delta z_m}}e^{-jk_z\Delta z_m}\quad(2D), \tag{13b}$$

$$\tilde{W}_0(\mathbf{k},\Delta z_m,\omega)=\frac{c/2}{\omega}\left(\frac{jk_z^2}{8\pi\Delta z_m}\right)e^{-jk_z\Delta z_m}\quad(3D), \tag{13c}$$

with

$$k_z=\sqrt{\left(\frac{c/2}{\omega}\right)^2-|\mathbf{k}|^2}\,.$$

Note that $\tilde{W}_0$ equals the convolution of $\tilde{W}^-$ with $\tilde{W}^+$ along $\mathbf{k}$ (Berkhout, 1985, Chap. VI).

Similar to the *multi*-offset situation, the bandlimited inverse operator for *zero*-offset data is given by

$$\tilde{F}_0(\mathbf{k},\Delta z_m,\omega)=\tilde{W}_0^{-1}(\mathbf{k},\Delta z_m,\omega)\quad\text{for }|\mathbf{k}|\leqslant\frac{\omega}{c/2}, \tag{14a}$$

$\tilde{W}_0$ being given by (13b) and (13c).

Using again the stationary phase approach for the inverse spatial Fourier transform we obtain

$$F_0(x,\Delta z_m,\omega)=-2je^{2jkr}\quad(2D), \tag{14b}$$

$$F_0(x,y,\Delta z_m,\omega)=-4e^{2jkr}\quad(3D). \tag{14c}$$

Note that these expressions represent one row of $\mathbf{F}_0(z_m,z_0)=[\mathbf{W}_0(z_0,z_m)]^{-1}$.

IV. IMAGE RESTORATION

Perfect imaging results require

$$\mathbf{W}^+(z_m,z_0)\mathbf{F}^+(z_0,z_m)=\mathbf{I},$$

$$\mathbf{F}^-(z_m,z_0)\mathbf{W}^-(z_0,z_m)=\mathbf{I}.$$

Unfortunately, these results can never be reached in practice. We mention two fundamental reasons:

(1) Due to the limited spatial bandwidth of propagation matrices $\mathbf{W}^+$ and $\mathbf{W}^-$, $\mathbf{F}^+$ and $\mathbf{F}^-$ do not exist and bandlimited versions must be used.

(2) Due to limitations of the macro model the propagation matrices $\overline{\mathbf{W}}^+$ and $\overline{\mathbf{W}}^-$ are not correct and the bandlimited inversion results will be further degraded, particularly by phase residuals.

Mathematically,

$$\mathbf{W}^+(z_m,z_0)\mathbf{F}^+(z_0,z_m)=\mathbf{E}^+(z_m), \tag{15a}$$

$$\mathbf{F}^-(z_m,z_0)\mathbf{W}^-(z_0,z_m)=\mathbf{E}^-(z_m), \tag{15b}$$

$\mathbf{F}^+$ and $\mathbf{F}^-$ being generally defined by (4b) and (4c).

If $\mathbf{S}^+(z_0)$ and $\mathbf{D}^-(z_0)$ cannot be represented by unity matrices, then

$$[\mathbf{W}^+(z_m,z_0)\mathbf{S}^+(z_0)]\mathbf{F}^+(z_0,z_m)=\mathbf{E}^+(z_m), \quad (16a)$$

$$\mathbf{F}^-(z_m,z_0)[\mathbf{D}^-(z_0)\mathbf{W}^-(z_0,z_m)]=\mathbf{E}^-(z_m). \quad (16b)$$

In (15) and (16) the bandlimited properties of $\mathbf{E}^+$ and $\mathbf{E}^-$ are determined by the bandlimited properties of $(\mathbf{W}^+,\mathbf{S}^+)$ and $(\mathbf{D}^-,\mathbf{W}^-)$ and the phase properties of $\mathbf{E}^+$ and $\mathbf{E}^-$ are determined by the phase differences between $(\mathbf{W}^+,\mathbf{W}^-)$ and $(\overline{\mathbf{W}}^+,\overline{\mathbf{W}}^-)$.

Note that in hypothetical situations $\mathbf{E}^+$ and $\mathbf{E}^-$ could be unity matrices, but in practice they always represent band matrices, causing so-called blurred images:

$$\hat{\mathbf{R}}(z_m)=\mathbf{E}^-(z_m)\mathbf{R}^+(z_m)\mathbf{E}^+(z_m) \quad (17a)$$

or

$$\hat{R}_{ij}^{+}(z_m)=\sum_k\sum_l E_{ik}^{-}(z_m)R_{kl}^{+}(z_m)E_{lj}^{+}(z_m) \quad (17b)$$

or, assuming a diagonal reflectivity matrix,

$$\hat{R}_{ii}^{+}(z_m)=\sum_j E_{ij}^{2}(z_m)R_{jj}^{+}(z_m) \quad (18a)$$

with

$$E_{ij}^{2}=E_{ij}^{-}E_{ji}^{+}. \quad (18b)$$

Equations (17) and (18) define the underlying equations for the restoration process in acoustical reflection imaging. Note that for laterally invariant media (18a) represents a lateral convolution process for each temporal frequency component.

V. IMAGING AS PART OF THE FULL INVERSION PROCESS

So far the influence of the surface was neglected and multiple scattering was ignored. In addition, it was assumed that we were interested in the diagonal reflection coefficients only. In the following reflection imaging will be set in a broader context, allowing an easy comparison between image formation and inversion techniques.

The full acoustical reflection inverse problem can be subdivided in three principal steps (Fig. 3).

A. Surface-related pre-processing [Fig. 4(a)]

The data at the surface $(z=z_0)$ are decomposed in down- and upgoing waves,

$$\mathbf{S}^+(z_0)=\mathbf{D}^+(z_0)\mathbf{S}(z_0), \quad (19a)$$

$$\mathbf{P}^-(z_0)=[\mathbf{D}^-(z_0)]^{-1}\mathbf{P}(z_0), \quad (19b)$$

the influence of the source properties are eliminated,

$$\mathbf{X}(z_0,z_0)=\mathbf{P}^-(z_0)[\mathbf{S}^+(z_0)]^{-1}, \quad (19c)$$

and, optionally, the influence of the surface reflectivity is removed

$$\mathbf{X}_0(z_0,z_0)=[\mathbf{I}+\mathbf{X}(z_0,z_0)\mathbf{R}^-(z_0)]^{-1}\mathbf{X}(z_0,z_0), \quad (19d)$$

see Eq. (14) in part I.

B. Elimination of propagation effects [Fig. 4(b)]

The propagation effects of medium slice (z_0,z_1) are eliminated,

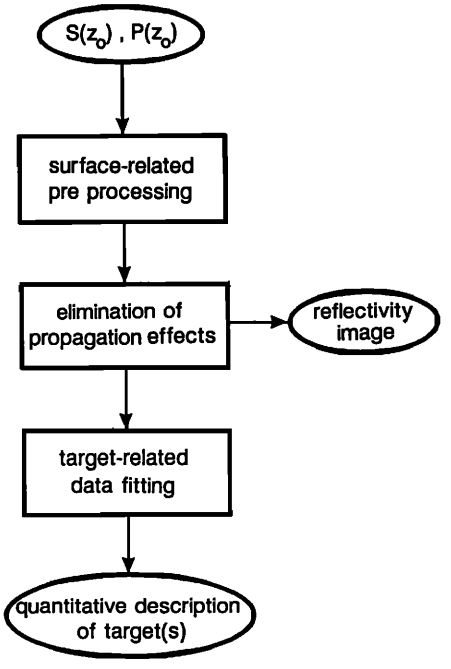

FIG. 3. Inversion of acoustic reflection measurements in terms of three steps.

$$\mathbf{X}(z_1,z_1)=\overline{\mathbf{F}}^-(z_1,z_0)\mathbf{X}_0(z_0,z_0)\overline{\mathbf{F}}^+(z_0,z_1) \quad (20a)$$

with

$$\overline{\mathbf{F}}^+(z_0,z_1)=[\overline{\mathbf{W}}^+(z_1,z_0)]^{-1}$$

and

$$\overline{\mathbf{F}}^-(z_1,z_0)=[\overline{\mathbf{W}}^-(z_0,z_1)]^{-1}$$

in some sense [see, e.g., (4b) and (4c)], the angle-dependent reflection coefficients at the new depth level $(z=z_1)$ are computed by Radon transformation at $t=0$:

$$\hat{\hat{R}}^+(x_i,z_1;p)=\frac{1}{N}\sum_n\left(\sum_k X_{ik}(z_1,z_1)e^{+j\omega_n(x_i-x_k)p}\right) \quad (20b)$$

and, optionally, the influence of the new surface reflectivity at $z=z_1$ is removed (internal scattering),

$$\mathbf{X}_0(z_1,z_1)=[\mathbf{I}+\mathbf{X}'(z_1,z_1)\hat{\mathbf{R}}^-(z_1)]^{-1}\mathbf{X}'(z_1,z_1), \quad (20c)$$

where

$$\hat{\mathbf{R}}^-(z_1)=-\hat{\mathbf{R}}^+(z_1),$$

$$\mathbf{X}'(z_1,z_1)=[\hat{\mathbf{T}}^-(z_1)]^{-1}[\mathbf{X}(z_1,z_1)-\hat{\mathbf{R}}^+(z_1)]\times[\hat{\mathbf{T}}^+(z_1)]^{-1},$$

$$\hat{\mathbf{T}}^+(z_1)=\mathbf{I}+\hat{\mathbf{R}}^+(z_1), \text{ and } \hat{\mathbf{T}}^-(z_1)=\mathbf{I}+\hat{\mathbf{R}}^-(z_1).$$

This step [Eqs. (20a), (20b), and optionally, (20c)] is repeated for all depth levels of interest.

C. Target data fitting [Fig. 4(c)]

The reflection information (output of step 2) is used to construct an initial model of the target. The initial model is updated via an optimization algorithm by matching the simulated target response with the actually measured target re-

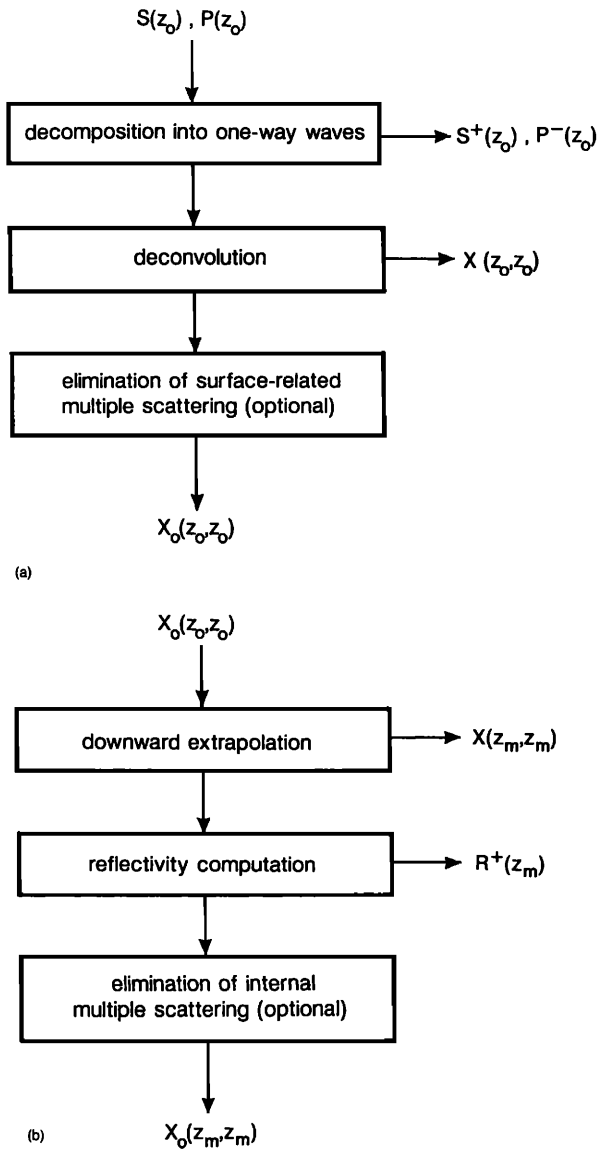

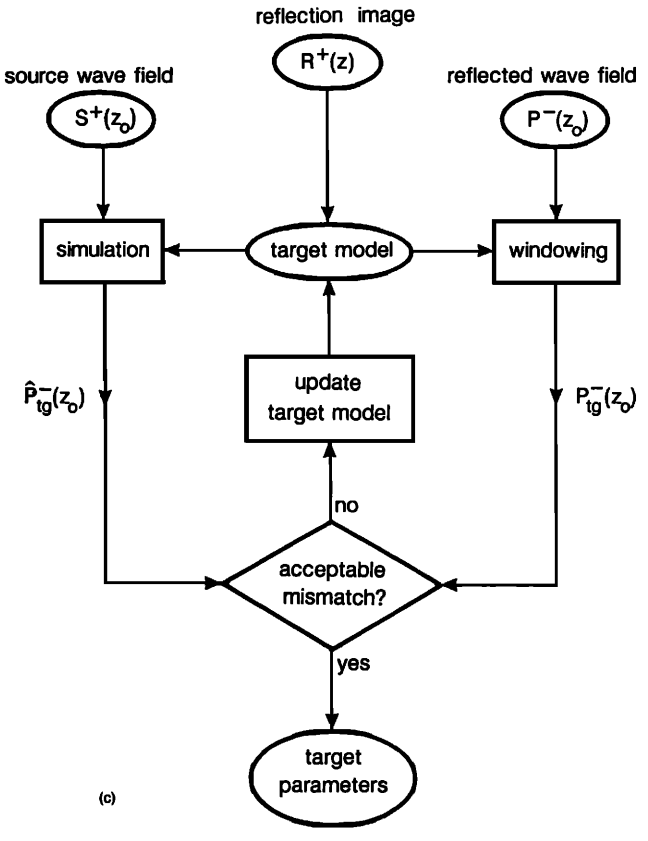

FIG. 4. (a) Surface-related pre-processing; (b) elimination of propagation effects (imaging); (c) target-related data fitting (characterization).

sponse. Nowadays there are many optimization algorithms available, but we prefer the so-called Gauss–Newton approach (see, e.g., Gill *et al.*, 1981). The model of the target is defined by *tissue*-oriented parameters (medical diagnostics), *defect*-oriented parameters (ultrasonic inspection) or *litho*-oriented parameters (seismic exploration). These discipline-oriented parameters need to be translated into velocity (c_p,c_s) and density information before simulation can start (Fig. 5). In the open literature very little attention is paid to this important translation problem.

From the aforegoing we may conclude that reflection imaging relates to step 2 in the inversion scheme, i.e., elimination of propagation effects, under the assumption that multiple scattering energy and transmission losses are neglected.

VI. CONCLUSIONS

(1) Acoustical reflection measurements are determined by the combination of *propagation* and *reflection* effects of the medium under investigation. Image formation can be seen as the process that *eliminates the propagation effects* from the measurements. The result is a spatial reflectivity

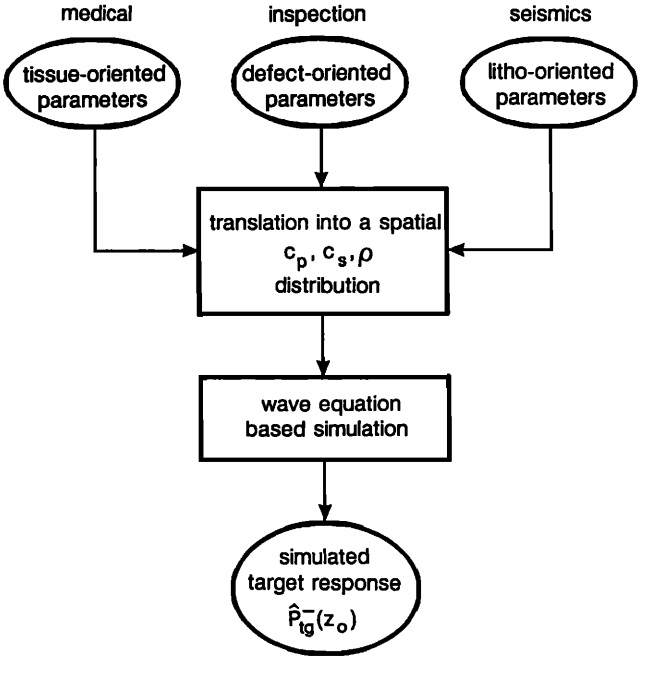

FIG. 5. Translation of the discipline-oriented model into an acoustic model.

distribution ("structural image"), yielding information on the local inhomogeneities.

(2) Mathematically, image formation can be formulated in terms of double *matrix inversion*; one inversion to compensate for the downward propagation matrix and one inversion to compensate for the upward propagation matrix.

(3) If *angle-dependent* reflectivity information is aimed for, then an extra process is required in terms of Radon transformation.

(4) Numerical image formation by double matrix inversion can be translated into a physical measurement process with double *focusing*; focusing is applied at emission to compensate for the downward propagation effects and focusing is applied at detection to compensate for the upward propagation effects.

(5) Numerical image formation for zero-offset (or pulse-echo) data can be formulated in terms of *single* matrix inversion. It is shown that for this type of data the inverse matrix elements define simple phase shifts only.

(6) Full acoustical reflection inversion can be described by three principal steps. In the first step the influence of the data acquisition surface is eliminated, including undesired source and detector properties. In the second step the propagation effects are eliminated, including multiple scattering. In the third step the reflectivity information is translated into material properties ("characterization").

Numerical image formation may be considered as a simplified version of the second step.

Berkhout, A. J. (**1985**). *Seismic Migration: Imaging of Acoustic Energy by Wave Field Extrapolation. A. Theoretical Aspects* (Elsevier, New York), 3rd ed.

Berkhout, A. J. (**1993**). "A unified approach to acoustical reflection imaging. I: The forward model," J. Acoust. Soc. Am. **93**, 2005–2016.

Gill, P. E., Murray, W., and Wright, M. H. (**1981**). *Practical Optimization* (Academic, New York).

Goustias, J. L., and Mendel, J. M. (**1987**). "Inverse problems in two-dimensional acoustic media: A linear imaging model," J. Acoust. Soc. Am. **81**, 1471–1485.

Tarantola, A. (**1987**). *Inverse Problem Theory: Methods for Data Fitting and Model Parameter Estimation* (Elsevier, New York).